Received: 29 January 2021 | Revised: 24 June 2021 | Accepted: 30 July 2021

DOI: 10.1002/alz.12456

Alzheimer's & Dementia®
THE JOURNAL OF THE ALZHEIMER'S ASSOCIATION

FEATURED ARTICLE

# Rates of longitudinal change in $^{18}$F-flortaucipir PET vary by brain region, cognitive impairment, and age in atypical Alzheimer's disease

**Jeffrey S. Phillips**[1] | **Frederick J. Nitchie IV**[1] | **Fulvio Da Re**[2] | **Christopher A. Olm**[1] | **Philip A. Cook**[1] | **Corey T. McMillan**[1] | **David J. Irwin**[1] | **James C. Gee**[1] | **Jacob G. Dubroff**[1] | **Murray Grossman**[1] | **Ilya M. Nasrallah**[1] | **for the Alzheimer's Disease Neuroimaging Initiative**[#]

[1] University of Pennsylvania, Philadelphia, Pennsylvania, USA

[2] University of Milan-Bicocca Faculty of Medicine and Surgery, Universita degli Studi di Milano-Bicocca Dipartimento di Medicina e Chirurgia, Milan, Italy

**Correspondence**
Jeffrey S. Phillips, 3400 Spruce St., 3 West Gates, Department of Neurology, Philadelphia, PA 19104, USA.
E-mail: Jeffrey.Phillips@pennmedicine.upenn.edu

[#]Data used in preparation of this article were obtained from the Alzheimer's Disease Neuroimaging Initiative (ADNI) database (adni.loni.usc.edu). As such, the investigators within the ADNI contributed to the design and implementation of ADNI and/or provided data but did not participate in analysis or writing of this report. A complete listing of ADNI investigators can be found at: http://adni.loni.usc.edu/wp-content/uploads/how_to_apply/ADNI_Acknowledgement_List.pdf.

**Funding information**
National Institute on Aging, Grant/Award Numbers: AG054519, AG017586, AG061277, AG066152, AG058732, AG066597, AG068057, AG063888, AG055005; National Institute of Neurological Disorders and Stroke, Grant/Award Numbers: NS109260, NS092091, NS107027; National Institute on Drug Abuse, Grant/Award Number: DA038726; the Alzheimer's Association, Grant/Award Number: AARF-16-443681; BrightFocus Foundation, Grant/Award Number: A2016244S; the Foundation of the American Society of Neuroradiology; the Commonwealth of Pennsylvania, and the Penn Institute on Aging; National Institutes of Health, Grant/Award Number: U01-AG024904

## Abstract

**Introduction:** Longitudinal positron emission tomography (PET) studies of tau accumulation in Alzheimer's disease (AD) have noted reduced increases or frank decreases in tau signal. We investigated how such reductions related to analytical confounds and disease progression markers in atypical AD.

**Methods:** We assessed regional and interindividual variation in longitudinal change on $^{18}$F-flortaucipir PET imaging in 24 amyloid beta (A$\beta$)+ patients with atypical, early-onset amnestic or non-amnestic AD plus 62 A$\beta$– and 132 A$\beta$+ Alzheimer's Disease Neuroimaging Initiative (ADNI) participants.

**Results:** In atypical AD, $^{18}$F-flortaucipir uptake slowed or declined over time in areas with high baseline signal and older, more impaired individuals. ADNI participants had reduced longitudinal change in early Braak stage regions relative to late-stage areas.

**Discussion:** Results suggested radioligand uptake plateaus or declines in advanced neurodegeneration. Further research should investigate whether results generalize to other radioligands and whether they relate to changes of the radioligand binding site structure or accessibility.

KEYWORDS
atypical Alzheimer's disease, flortaucipir, logopenic-variant primary progressive aphasia, longitudinal, non-amnestic Alzheimer's disease, positron emission tomography, posterior cortical atrophy, tau

This is an open access article under the terms of the Creative Commons Attribution-NonCommercial-NoDerivs License, which permits use and distribution in any medium, provided the original work is properly cited, the use is non-commercial and no modifications or adaptations are made.
© 2021 The Authors. *Alzheimer's & Dementia* published by Wiley Periodicals LLC on behalf of Alzheimer's Association.

## 1 | INTRODUCTION

Tau imaging with positron emission tomography (PET) is an important biomarker of Alzheimer's disease (AD) neuropathologic change[1] and clinical trial endpoints.[2] Straightforward interpretation of tau PET results may assume that tracer uptake increases linearly with disease progression. However, extant studies provide an incomplete picture of tau PET signal change over time. Multiple studies have attributed regional slowing[3] of or decreases[4,5] in tracer retention to measurement error or processing artifacts. While skepticism regarding apparent tau reductions is appropriate, radioligand uptake could behave nonlinearly over the disease course due to valid biologic changes, as illustrated by sigmoidal models of AD biomarker trajectories.[6,7] First, tau pathology burden may plateau or decrease in advanced disease due to limiting factors like the tissue's capacity for retaining pathologic aggregates.[8] Alternatively, biologic changes may affect tracer binding to tau aggregates. Indeed $^{18}$F-flortaucipir binds differentially to immature versus mature tau[9] and to different tau species isolated from cerebrospinal fluid (CSF).[10] Changes in both tissue burden and tracer binding could cause the tau PET signal to vary between individuals and regionally within individuals based on the progression of AD pathology.

Atypical AD, which encompasses both non-amnestic and early-onset amnestic variants, provides a unique context for investigating longitudinal change in tau PET imaging. Because atypical AD patients have greater neocortical tau burden and less hippocampal tau in histopathological examinations,[11] tau PET quantification may be less confounded by artifacts related to region segmentation or choroid plexus off-target binding,[9] which affect measurement accuracy in early-stage regions for typical AD, including the hippocampus.[12] Magnetic resonance imaging (MRI) and PET studies have consistently demonstrated differing patterns of disease spread between atypical and typical, amnestic patients,[13–16] with distinct neocortical disease foci in logopenic-variant primary progressive aphasia (lvPPA), posterior cortical atrophy (PCA), corticobasal syndrome (CBS), behavioral/dysexecutive AD (bvAD; note mixed findings regarding atrophy in bvAD,[17]) and early-onset amnestic AD[18] (aAD). Few longitudinal studies[15,16] have investigated atypical or non-amnestic syndromes (which are prevalent in early-onset AD[19,20]) in a manner that clearly links radioligand uptake to patient phenotype. Compared to typical AD, atypical cases also exhibit cognitive and functional impairment at an earlier age.[21] These features facilitate imaging of tau accumulation across a greater volume of the brain and a larger temporal window than in typical, later-onset amnestic cases, in which neocortical disease is limited to Braak stages IV–VI.[22]

In the present study, we investigated apparent slowing of or decreases in longitudinal $^{18}$F-flortaucipir signal in atypical AD patients from the University of Pennsylvania's Frontotemporal Degeneration Center (FTDC). We aimed to ascertain whether such changes were more likely attributable to measurement error, including processing artifacts and random statistical noise, or were consistent with expected biologic change in atypical AD. We hypothesized that regions of early disease would display high baseline $^{18}$F-flortaucipir signal but longitudinal slowing or reductions of tracer binding, while late-stage disease regions would display lower baseline tau and greater subsequent increases. Furthermore, we predicted that tau signal changes would vary between patients according to disease severity and age, with more advanced cases exhibiting reduced longitudinal change relative to milder cases. We also assessed the generalizability of these analyses to typical AD by analyzing longitudinal $^{18}$F-flortaucipir data in a larger sample of Alzheimer's Disease Neuroimaging Initiative (ADNI) participants.

### HIGHLIGHTS

- We assessed tau positron emission tomography (PET) change over time in atypical, early-onset, and non-amnestic Alzheimer's disease.
- Areas of early atrophy showed reduced change, including net decreases.
- Older and more impaired patients were more likely to exhibit PET decreases over time.
- Regression to the mean and atrophy could not explain observed PET decreases.
- Results suggest that tau PET signal may plateau or decline in advanced disease.

### RESEARCH IN CONTEXT

1. **Systematic review**: We used PubMed to review longitudinal tau positron emission tomography (PET) imaging studies of Alzheimer's disease (AD) spectrum patients for reports or discussion of plateauing of or decreases in longitudinal tracer uptake. High-profile studies to date have acknowledged longitudinal decreases in a subset of participants or brain areas but have not systematically investigated whether such effects are the result of technical and random statistical error versus correlates of AD pathologic change.
2. **Interpretation**: We found that longitudinal decreases in tau PET signal did not occur randomly but rather in brain areas and individuals with advanced disease. Our findings in atypical AD patients are consistent with prior work showing reduced tau in the cerebrospinal fluid of such patients and challenge the assumption that tau biomarkers will increase linearly across the disease course.
3. **Future directions**: Further research should investigate factors that may influence PET signal change, including changes in tau conformation and aggregation state from early to late disease.

## 2 | METHODS

### 2.1 | Participant selection and diagnosis

Atypical AD patients were recruited through the Cognitive Neurology Clinic at the Hospital of the University of Pennsylvania. Participants or caregivers gave informed consent according to the Declaration of Helsinki. Inclusion criteria included amyloid positivity according to CSF assay or PET imaging, two $^{18}$F-flortaucipir PET scans, two isotropic T1-weighted 3-Tesla MRI scans, and a non-amnestic or early-onset amnestic syndrome. Exclusion criteria included significant vascular disease, other psychiatric or neurological disease, traumatic brain injury, or substance abuse. CSF samples were processed according to published methods,[23] and amyloid positivity was based on an autopsy-validated amyloid beta ($A\beta)_{1\text{-}42}$ concentration < 168 pg/mL.[24] This conservative threshold minimized the risk of including patients with primary frontotemporal lobar degeneration (FTLD) and secondary AD neuropathologic change. In participants with $^{18}$F-florbetaben PET, a visual read by a trained radiologist (IMN) determined A$\beta$ positivity. Two participants were excluded for excessive motion. All patients were clinically diagnosed by consensus of board-certified neurologists (DI and MG). Phenotypic syndrome was diagnosed using accepted criteria for lvPPA,[25,26] PCA,[27] bvAD,[28] CBS,[29–32] and aAD.[33] One patient with impairments in executive and visuospatial function but preserved memory was diagnosed with non-amnestic mild cognitive impairment (naMCI).[33,34] Baseline data for eight participants were previously reported.[35,36] Cognition was evaluated by total score on the Mini-Mental State Examination (MMSE)[37] and Clinical Dementia Rating (CDR) scale modified for FTLD, hereafter FTLD-CDR;[38] the latter measure includes the CDR sum of boxes plus assessments of behavior and language relevant for assessment of non-amnestic AD.

Data obtained from the ADNI database (adni.loni.usc.edu) were used to investigate atypical AD findings in a larger sample with more typical, amnestic presentations. We selected ADNI participants with two $^{18}$F-flortaucipir PET scans either a CSF $A\beta_{1\text{-}42}$ concentration < 192 pg/mL or a positive amyloid PET scan. For individuals with more than two tau scans, we selected the first and last available. The ADNI sample comprised 69 amyloid-positive cognitively normal (CN) participants, 42 with MCI, and 21 with dementia at first PET scan (Table 1). As a control group, we included 62 amyloid-negative CN participants. Cognitive function was assessed by MMSE total score and CDR sum of boxes.[39]

### 2.2 | Neuroimaging methods

$^{18}$F-flortaucipir data for atypical AD patients were acquired on a Philips Ingenuity TF PET/CT scanner between February 2015 and January 2020. Participants were injected intravenously with 10 mCi (370 MBq) ± 20% $^{18}$F-flortaucipir; two sub-threshold doses (5.9 and 7.7 mCi) were approved by the injecting radiologist. Participants were imaged in 5-minute frames 75 to 105 minutes post-injection; images were reconstructed with 2 mm isotropic voxels and a 256 mm field of view. PET data were corrected for scatter, signal attenuation, and head motion, then averaged across frames. T1-weighted MRI data were acquired on a Siemens 3-Tesla scanner with 1 mm isotropic voxels. Using the Advanced Normalization Tools (ANTs) longitudinal MRI pipeline, previously described in detail,[40] we segmented each MRI image based on priors for CSF, deep and cortical gray matter, white matter, brainstem, and cerebellum; and created a temporally unbiased reference image for each participant as an intermediate registration target. This procedure reduces variability in tissue segmentation and structural metrics.[41] The mean PET image was aligned with each T1-weighted MRI timepoint using a rigid-body registration, and standardized uptake value ratio (SUVR) maps (Figure 1) were created by dividing each voxel by mean intensity in a cerebellar reference region that excluded deep gray nuclei and core white matter (Figure A.8 in supporting information).[42,43] Longitudinal change was quantified by subtracting SUVRs for the baseline scan ($SUVR_{base}$) from follow-up values and dividing by inter-scan interval to estimate annualized change (ΔSUVR). Outlier correction of $SUVR_{base}$ and ΔSUVR censored observations that were >3 SD from the grand mean, excluding 19 of 5256 regional observations for $SUVR_{base}$ (0.4%) and 44 (0.8%) for ΔSUVR. We report results with and without partial volume correction (PVC) using the iterative Yang method from the PETPVC toolbox.[44] In supplementary analyses, we computed SUVRs relative to an eroded white matter region (Figure A.1 in supporting information). Gray matter volume and mean $^{18}$F-flortaucipir SUVR were computed for 219 anatomical labels in Hagmann et al.'s cortical parcellation.[45,46] The average interval between MRI and PET was 30.1 days (standard deviation [SD]: 63.5; range: −151 to 168); the interval between baseline and follow-up $^{18}$F-flortaucipir scans was 1.64 years (SD: 0.85; range: 0.9 to 3.6).

To characterize regions of interest (ROIs) as areas of earlier versus later disease in the atypical AD sample, we computed phenotype-specific models of regional atrophy progression (Figure 2) in a separate cross-sectional sample of 3-Tesla, T1-weighted MRI scans (Table A.2 in supporting information) using an approach based on Phillips et al.[13] We assumed that sites of early neurodegeneration would be atrophied in all or most participants, and areas of later disease in a smaller subset. Atrophy was quantified by computing W-scores correcting for age and intracranial volume.[47] The resulting models distinguished five stages of cortical disease in each phenotype (1 = earliest ROIs involved; 5 = latest ROIs; details are in the supporting information). These values represent a hypothetical sequence of cortical disease spread and are not equivalent to Braak staging.

For ADNI participants, we analyzed $^{18}$F-flortaucipir SUVR data published in the ADNI repository by researchers at the University of California, Berkeley (UCBERKELEYAV1451_01_14_21 and UCBERKELEYAV1451_PVC_01_15_21 tables, downloaded May 23, 2021). We analyzed data both with and without PVC using the approach implemented by Baker et al.[12] For each participant, all PET images were registered to the baseline MRI and resampled to uniform resolution. SUVRs were computed for cortical and deep gray matter ROIs using

**TABLE 1** Participant characteristics from atypical AD (top) and ADNI (bottom) samples, summarized by phenotype

| | N | Sex | Age (y) | Education (y) | MMSE | FTLD-CDR/ CDR SoB | Follow up interval (y) | Baseline global SUVR | Annual SUVR change |
|---|---|---|---|---|---|---|---|---|---|
| | Atypical Alzheimer's disease sample | | | | | | | | |
| lvPPA | 8 | 5 (62.5) | 60.5 [58.0, 64.0] | 17.0 [13.5, 20.0] | 24.5 [20.0, 27.3] | 5.5 [2.5, 5.8] | 1.39 [1.25, 1.92] | 1.62 [1.58, 1.74] | 0.075 [0.033, 0.110] |
| PCA | 8 | 3 (37.5) | 61.0 [59.8, 63.3] | 16.0 [15.0, 18.0] | 25.0 [24.0, 27.3] | 3.0 [3.0, 3.4] | 1.16 [0.98, 2.77] | 1.70 [1.62, 1.88] | 0.067 [0.026, 0.076] |
| CBS | 3 | 3 (100.0) | 67.0 [58.0, 69.0] | 16.0 [14.0, 17.0] | 24.0 [20.0, 25.5] | 6.5 [6.0, 8.5] | 0.93 [0.89, 0.96] | 1.95 [1.70, 2.09] | 0.032 [−0.050, 0.117] |
| aAD | 3 | 1 (33.3) | 58.0 [55.5, 65.5] | 18.0 [18.0, 19.0] | 23.0 [22.5, 25.0] | 4.750 [4.1, 5.4] | 2.30 [1.73, 2.60] | 1.66 [1.42, 1.71] | 0.023 [0.022, 0.061] |
| bvAD | 1 | 0 (0.0) | 75.0 [75.0, 75.0] | 18.0 [18.0, 18.0] | 23.0 [23.0, 23.0] | 9.0 [9.0, 9.0] | 1.079 [1.08, 1.08] | 1.92 [1.92, 1.92] | −0.069 [−0.069, −0.069] |
| naMCI | 1 | 1 (100.0) | 58.0 [58.0, 58.0] | 16.0 [16.0, 16.0] | 21.0 [21.0, 21.0] | 3.0 [3.0, 3.0] | 1.11 [1.11, 1.11] | 2.05 [2.05, 2.05] | 0.032 [0.032, 0.032] |
| p | | 0.286 | 0.433 | 0.737 | 0.812 | 0.06 | 0.567 | 0.347 | 0.551 |
| | ADNI sample | | | | | | | | |
| CN Aß− | 62 | 34 (54.8) | 72.1 [69.2, 76.9] | 16.0 [14.3, 18.0] | 29.0 [29.0, 30.0] | 0.0 [0.0, 0.0] | 1.97 [1.25, 2.16] | 1.05 [1.02, 1.09] | 0.005 [−0.011, 0.017] |
| CN Aß+ | 69 | 37 (53.6) | 76.379 [71.0, 81.3] | 18.0 [16.0, 18.0] | 29.0 [28.0, 30.0] | 0.0 [0.0, 0.0] | 1.85 [1.05, 2.03] | 1.08 [1.02, 1.14] | 0.003 [−0.011, 0.024] |
| MCI | 42 | 19 (45.2) | 77.2 [70.6, 79.9] | 16.0 [14.0, 19.0] | 27.0 [26.0, 29.0] | 1.0 [0.5, 1.5] | 1.36 [1.03, 2.09] | 1.13 [1.07, 1.22] | 0.008 [−0.007, 0.029] |
| Dementia | 21 | 9 (42.9) | 80.1 [71.8, 82.9] | 15.0 [13.0, 16.0] | 22.0 [20.0, 25.0] | 5.0 [4.5, 5.5] | 1.17 [1.01, 1.84] | 1.16 [1.08, 1.43] | 0.007 [−0.016, 0.020] |
| p | | 0.643 | 0.0947 | 0.007 | <0.001 | <0.001 | 0.149 | <0.001 | 0.891 |

Notes: For the atypical AD sample, global SUVR is the mean over cortical gray matter. For the ADNI sample, global SUVR is the volume-weighted mean over Braak I, III/IV, and V/VI regions. Change in SUVR: annualized change between baseline and follow-up scans. For atypical AD participants, CDR sum of boxes plus total score on the FTLD language and behavior supplements is given; for ADNI participants, CDR sum of boxes is reported.

Abbreviations: aAD, early-onset amnestic AD; Aß+/−, positive or negative for amyloid-beta biomarkers; AD, Alzheimer's disease; ADNI, Alzheimer's Disease Neuroimaging Initiative; bvAD, behavioral/dysexecutive AD; CBS, corticobasal syndrome; CDR, Clinical Dementia Rating; CN, cognitively normal; FTLD, frontotemporal lobar degeneration; lvPPA, logopenic-variant primary progressive aphasia; MCI, mild cognitive impairment; MMSE, Mini-Mental State Examination; naMCI, non-amnestic mild cognitive impairment; PCA, posterior cortical atrophy; SUVR, standardized uptake value ratio.

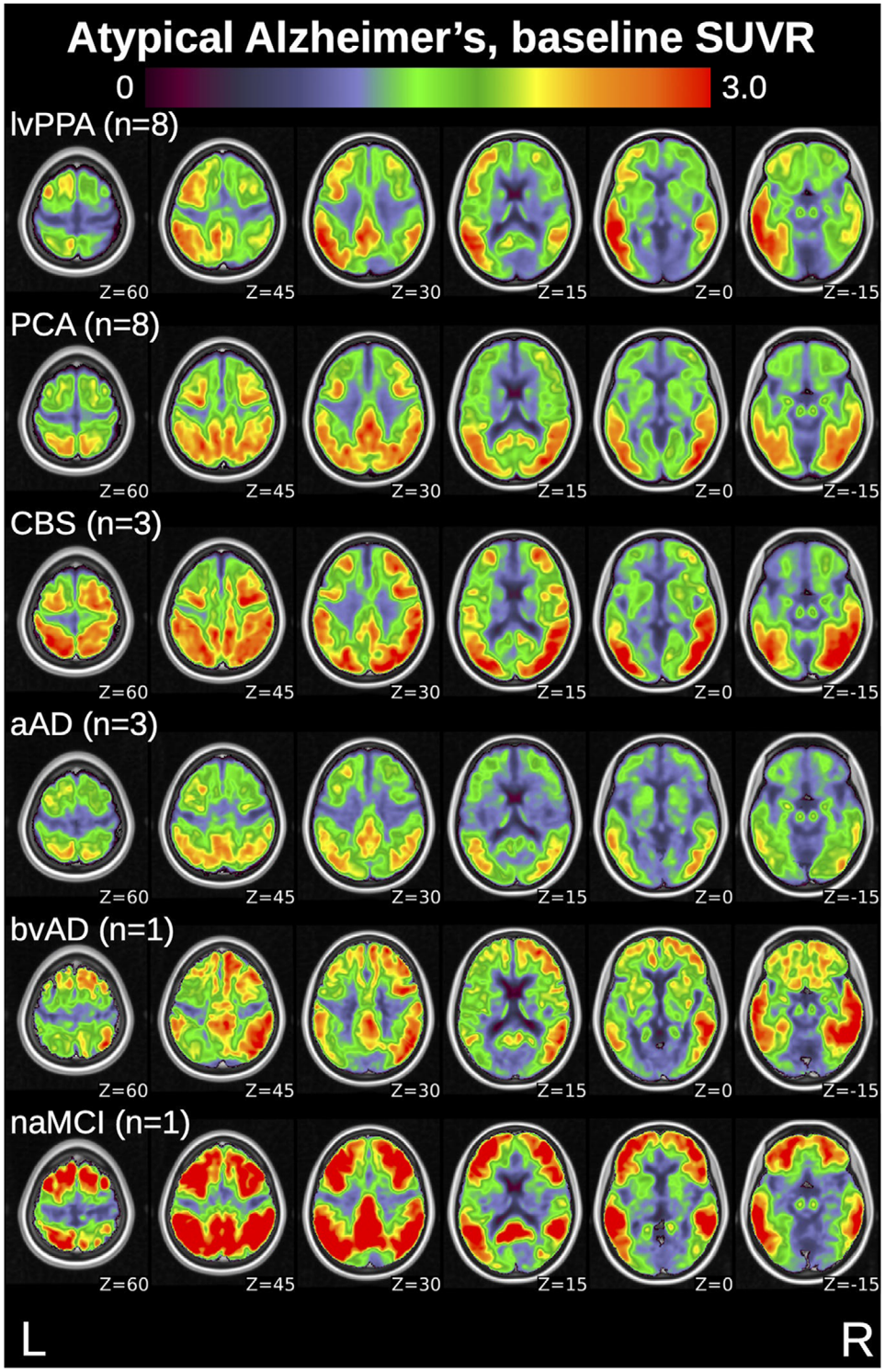


**FIGURE 1** Maps of uncorrected baseline $^{18}$F-flortaucipir standardized uptake value ratio (SUVR) for the atypical Alzheimer's disease (AD) sample, averaged by initial clinical presentation. All maps are displayed in Montreal Neurological Institute (MNI) template space. Image left is anatomical left

FreeSurfer 7.1.1. SUVRs were re-normalized to inferior cerebellar gray matter; volume-weighted averages were computed for global signal plus Braak stage I, III/IV, and V/VI meta-ROIs. Landau et al.'s analysis omits the hippocampus (Braak II) due to signal contamination from the choroid plexus.[48]

## 2.3 | Statistical analysis

Table 1 reports mean cortical $SUVR_{base}$ and $\Delta SUVR$ for atypical AD patients; and global mean $SUVR_{base}$ and mean $SUVR_{base}$ in a meta-temporal ROI in the ADNI sample. We used linear regression

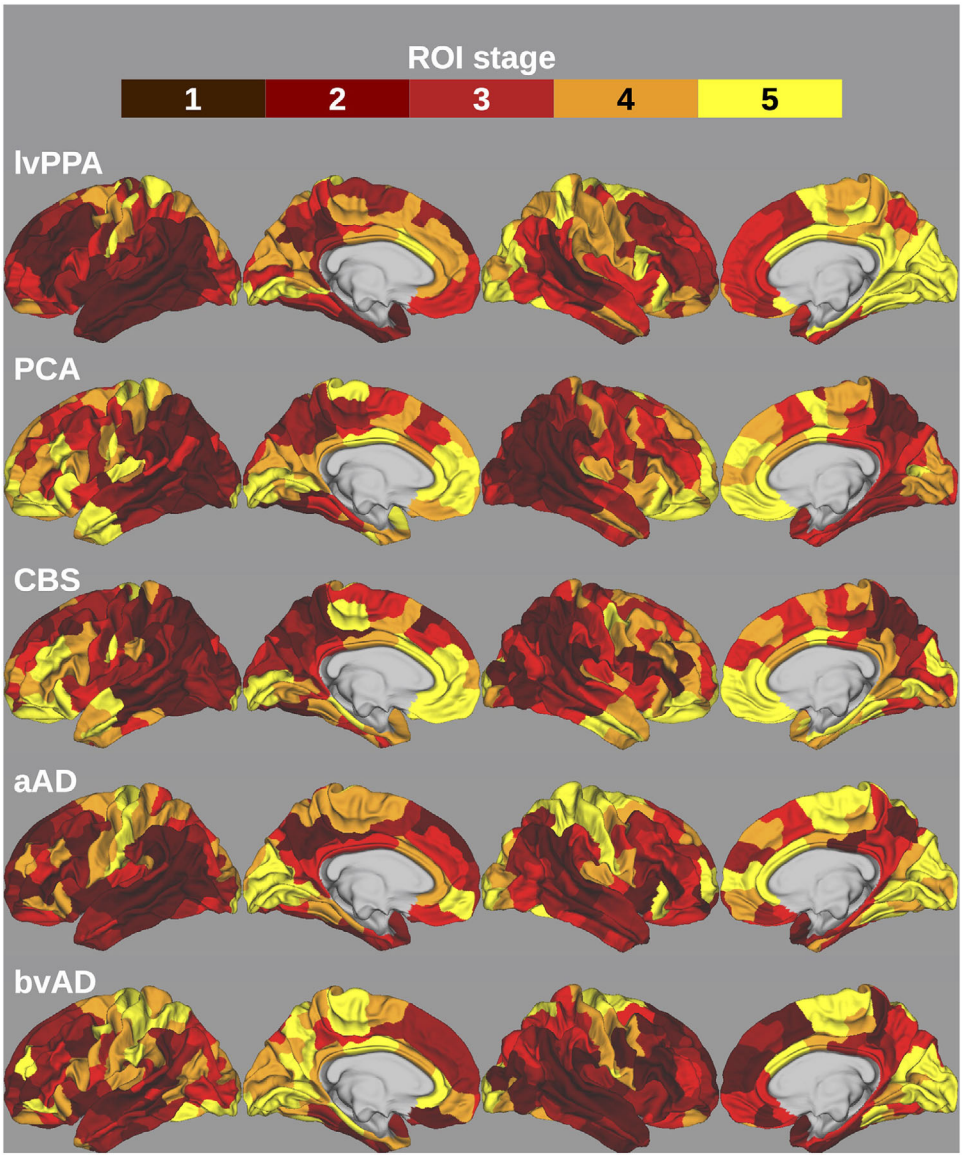


**FIGURE 2** Models of neocortical disease progression in atypical Alzheimer's disease, based on frequency of gray matter atrophy in an independent sample of patients. Stage 1 = earliest areas of disease; stage 5 = latest areas of disease

models adjusting for age and sex to assess between-group differences in the ADNI data. Next, we analyzed regional SUVRs using linear mixed effects (LME) models with a random intercept per person. To quantify agreement between observed and expected regional disease burden in atypical AD, Model 1 related baseline SUVR (hereafter, $SUVR_{base}$) to regional disease stages estimated from MRI-based models of atrophy progression (Figure 2), where stage 1 indicated regions of early disease and stage 5 indicated the latest involvement. We hypothesized early-stage ROIs would show higher tau burden than late-stage ROIs. Model 2 similarly related ΔSUVR to ROI stage; we hypothesized ROIs involved in early disease would show reduced longitudinal change relative to ROIs involved in later disease. Model 3 used polynomial regression to assess apparent quadratic trends in the relationship between ΔSUVR and $SUVR_{base}$. From visual inspection of regional SUVR change data, we hypothesized an inverted U-shaped relationship, according to which longitudinal SUVR increases would be low for regions with low $SUVR_{base}$, high for regions with moderate $SUVR_{base}$, and again reduced for regions with high $SUVR_{base}$. The supporting information additionally reports cubic b-spline models assessing the relationship between ΔSUVR and $SUVR_{base}$. Model 4 predicted ΔSUVR on the basis of a linear effect of $SUVR_{base}$ alone; we hypothesized that Model 3 would provide a better fit to the observed ΔSUVR data than this simpler model. Finally, to assess whether non-linear associations between ΔSUVR and $SUVR_{base}$ could be explained by gray matter atrophy, Model 5 predicted ΔSUVR from W-score measures of baseline and longitudinal gray matter atrophy. We hypothesized that this model would not explain observed ΔSUVR as well as Model 3. In the ADNI sample, we repeated these five models, adding a fixed factor of amyloid positivity and interaction terms between amyloid status and each other fixed factor (supporting information, Section 3). A significance threshold of $P < .05$ was applied to all group-level models. The supporting information reports single-subject implementations of these models

incorporating only fixed effects to assess the consistency of results on the individual level (Section 5), using a threshold of $P < .05$ after false discovery rate (FDR) correction for the number of participants in each sample.

We also addressed the possibility that longitudinal signal decreases in regions with high $SUVR_{base}$ could result from regression to the mean (RTM),[49] an often-overlooked statistical phenomenon that can create spurious signal changes in longitudinal designs. Hypothetical RTM effects could occur if certain brain areas exhibited a high $SUVR_{base}$ due to random error; follow-up measurements of the same brain areas would likely fall closer to the mean of the distribution, creating an apparent signal decrease. Lower correlation between two sets of observations leads to larger RTM effects.[50] We estimated RTM using a bootstrapping method to create simulated baseline and follow-up SUVR distributions with the same means, standard deviations, skewness, and mutual correlation as the original data; see supporting information, Section 9 for details.

## 3 | RESULTS

### 3.1 | Participant characteristics

The atypical AD sample (Table 1, top) included eight lvPPA, eight PCA, three CBS, one bvAD, one naMCI, and three aAD participants; for succinctness, the naMCI patient is included in references to atypical or non-amnestic AD. In the ADNI sample (Table 1, bottom), education, MMSE score, and CDR sum of boxes differed across CN, MCI, and dementia groups (all $P < .05$). Atypical AD patients were younger than ADNI participants in the CN amyloid-negative ($T[38] = -8.0$, $P < .0001$), CN amyloid-positive ($T[44] = -9.3$, $P < .0001$), MCI ($T[55] = -8.2$, $P < .0001$), and dementia ($T[33] = -6.2$, $P < .0001$) groups. MMSE scores in the atypical AD sample were significantly lower than those of the ADNI CN amyloid-negative ($T[24] = -6.4$, $P < .0001$), CN amyloid-positive ($T[25] = -5.8$, $P < .0001$), and MCI ($T[32] = -3.8$, $P = .0006$) groups but not the dementia group ($T[42] = 1.8$, $P = .0820$). Atypical AD participants did not differ from any of the ADNI groups in either education (all $T \leq 1.8$, $P > .08$) or sex ratio (all $\chi^2 \leq 1.9, P > .29$).

### 3.2 | Global tau burden

In atypical AD, mean cortical $SUVR_{base}$ ranged from 1.17 to 2.24 and did not differ by phenotype (Table 1). Mean cortical ΔSUVR exceeded zero (mean: 0.05; SD: 0.07; $T[23] = 3.7$, $P < .0001$) and did not differ by phenotype ($P = .63$). In the ADNI sample, global $SUVR_{base}$ was significantly higher than amyloid-negative controls for the MCI ($T[178] = 3.90$, $P < .0001$) and dementia ($T[178] = 7.19$, $P < .0001$) groups but not for amyloid-positive controls (Table A.3 in supporting information). Similar results were observed for meta-temporal SUVR (Table A.4 in supporting information) and for ADNI data processed using the atypical AD data pipeline (Section 10 in supporting information). Global ΔSUVR (Table A.5 in supporting information) was not significantly different from zero in any of the ADNI groups (all $P > .15$) and did not differ between ADNI groups ($F[3,188] = 0.21$, $P = .89$). In the meta-temporal ROI, ΔSUVR (Table A.6 in supporting information) exceeded zero for all groups except the dementia group (Table A.7 in supporting information). All ADNI groups had significantly lower global $SUVR_{base}$ (all $P < .002$) and ΔSUVR (all $P < .03$) than the atypical AD sample.

### 3.3 | Phenotypic variability in tau accumulation

Baseline $^{18}$F-flortaucipir results (Figure 1) varied according to phenotypic disease patterns,[16,35] including left-lateralized tracer uptake in lvPPA, posterior parietal and occipito-temporal uptake in PCA, and bilateral accumulation in CBS that extended into sensorimotor and prefrontal cortices. These results echoed atrophy analyses indicating lower W-scores for early versus late-stage regions (Figure A.9, Table A.34 in supporting information). According to Model 1, ROI stage was inversely associated with $SUVR_{base}$ ($\beta = -0.1977$, $T[95] = -20.50$, $P < .0001$), confirming that early-stage ROIs for each phenotype had higher $SUVR_{base}$ than later-stage ROIs (Figure 3). This negative association was similarly significant in analysis of PVC data ($\beta = -0.2941$, $T[95] = -20.44$, $P < .0001$). In contrast, the association between ROI stage and ΔSUVR (Model 2) was less robust ($\beta = 0.0072$, $T[95] = 3.64$, $P = .0004$) and did not survive PVC ($\beta = -0.00005$, $T[95] = -0.01$, $P = .9881$). The weakness of this group effect appeared to reflect inter-individual heterogeneity: in PVC analyses, 7 of 24 patients exhibited a positive association between ROI stage and ΔSUVR, while 10 of 24 individuals exhibited a negative association (Tables A.2–A.3 in supporting information).

In the ADNI sample, Braak stage was negatively associated with uncorrected $SUVR_{base}$ ($\beta = -0.0396$, $T[372] = -5.01$, $P < .0001$; Figure 3E). Amyloid-positive participants had higher $SUVR_{base}$ values than amyloid-negative controls ($\beta = 0.1452$, $T[192] = 4.47$, $P < .0001$) and a more negative slope of association between Braak stage and $SUVR_{base}$ ($\beta = -0.0208$, $T[372] = -2.17$, $P = .0308$). In model 2, amyloid positivity was associated with lower ΔSUVR values relative to amyloid-negative controls for uncorrected SUVR data ($\beta = 0.0072$, $T[377] = 2.72$, $P = .0068$). The main effect of ROI stage was non-significant ($P > .12$), but an interaction of amyloid status with Braak stage indicated that amyloid-positive individuals had reduced ΔSUVR for early Braak-stage regions relative to areas of later involvement ($\beta = 0.0189$, $T[374] = 2.60$, $P = .0096$). PVC results for Models 1 and 2 were consistent with uncorrected SUVRs (Figure 3F and H; Tables A.14–A.15 in supporting information).

### 3.4 | Association between regional baseline SUVR and subsequent change

We next investigated how regional $SUVR_{base}$ predicted ΔSUVR (Figure 4). Among atypical AD patients, higher $SUVR_{base}$ predicted higher

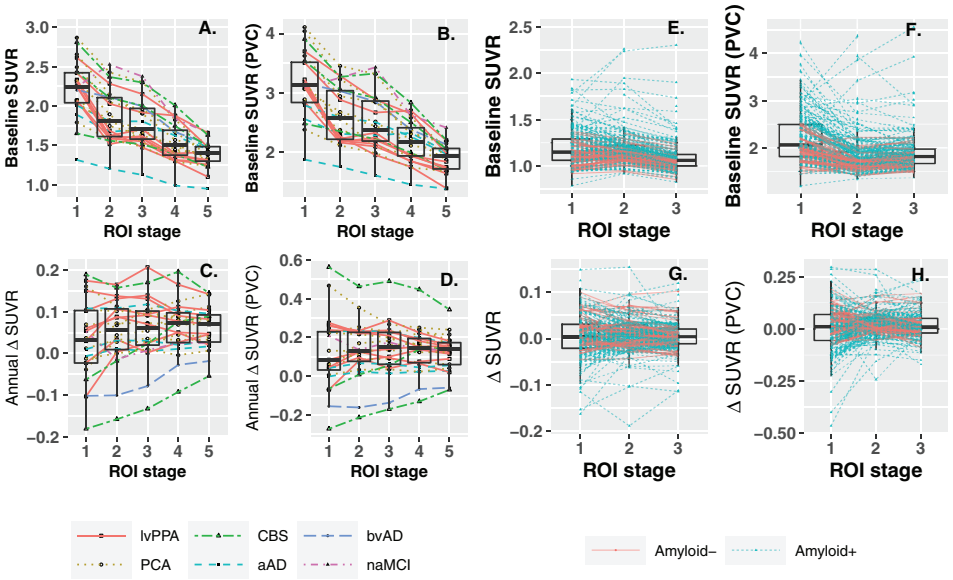


**FIGURE 3** Associations between regional stage of involvement, baseline standardized uptake value ratio (SUVR), and annual SUVR change for atypical Alzheimer's disease (AD) and Alzheimer's Disease Neuroimaging Initiative (ADNI) participants. A–D, left: atypical AD participants; E–H, right: ADNI participants. A, E, association between region of interest (ROI) stage and uncorrected SUVR at baseline. B, F, ROI stage versus baseline partial-volume-corrected SUVRs. C, G, ROI stage versus annualized longitudinal change in uncorrected SUVRs. D, H, ROI stage versus annualized longitudinal change in partial-volume-corrected SUVRs. Each data point represents the volume-weighted average over all ROIs of a given stage for a single participant. For ADNI participants, Stage 1 = Braak I; stage 2 = Braak III/IV; stage 3 = Braak V/VI

ΔSUVR ($\beta$ = 0.3243, T[5168] = 30.12, $P$ < .0001). At the same time, $SUVR_{base}{}^2$ was negatively associated with subsequent change ($\beta$ = −0.0907, T[5168] = −33.58, $P$ < .0001); this quadratic term accounted for observed ΔSUVR reductions by applying an exponentially larger decrement to brain areas with the highest $SUVR_{base}$. Similar effects were observed in PVC data and in individual models (Tables A.4, A.5, and A.11 in supporting information). Higher $SUVR_{base}$ thus predicted further increase in most regions and individuals; however, change was slowed or reversed in areas of highest baseline uptake. A paired $t$ test on squared residuals indicated Model 3 was more accurate than Model 4 (mean difference = 0.0012, T[5193] = 13.3, $P$ < .0001). A cubic spline model provided comparable performance to Model 3 (Table A.25 in supporting information).

In the ADNI sample, Model 3 indicated lower ΔSUVR values for amyloid-positive participants ($\beta$ = −0.126, T[192] = −3.72, $P$ = .0003). As in atypical AD, a positive linear effect of $SUVR_{base}$ ($\beta$= 0.218, T[12958] = 3.55, $P$ = .0004) and a negative quadratic effect ($\beta$= −0.096, T[12958] = −3.41, $P$ = .0007) were observed for amyloid-positive participants, while the opposite pattern was indicated for amyloid-negative controls (Table A.16 in supporting information). However, these effects did not survive PVC, and Model 3 results were not more accurate than the simpler Model 4 (mean difference = 0.0000, T[13155] = 1.4, $P$ = .161). In Model 4, amyloid-positive participants exhibited a positive slope of association between $SUVR_{base}$ and ΔSUVR ($\beta$ = 0.0190, T[12961] = 3.29, $P$ = .0010), indicating greater longitudinal increases for regions with higher $SUVR_{base}$ (Table A.17 in supporting information). On the individual level, 45 of 194 participants exhibited the same trend as on the group level; however, nearly as many (n = 40) exhibited a negative association between ΔSUVR and $SUVR_{base}$ (Table A.35 in supporting information).

## 4 | INTER-INDIVIDUAL DIFFERENCES IN LONGITUDINAL SUVR CHANGE

We hypothesized that ΔSUVR would vary according to individuals' disease severity and age, factors potentially associated with tau aggregate burden and maturity. We correlated patient-specific random intercepts from Model 3 with global cognitive impairment and age at time of first scan (Figure 5). Atypical AD patients with higher FTLD-CDR scores, indicating greater impairment, had reduced ΔSUVR relative to less impaired patients; similarly, older patients had reduced longitudinal change relative to younger patients. MMSE was not correlated with model intercepts, although the apparent trend was consistent with FTLD-CDR results. In the ADNI sample, Model 3 random intercepts were correlated with age ($P$ < .03; Figure 5, lower right) but not MMSE ($P$ > .22) or CDR sum of boxes ($P$ > .36).

### 4.1 | Secondary analysis of potential confound effects on longitudinal SUVR change

All regions exhibiting longitudinal decreases in the atypical AD analysis exceeded estimated regression to the mean (Section 9 in supporting information). Including atrophy covariates in Models 1–3 did not affect associations with ROI stage or associations between ΔSUVR and

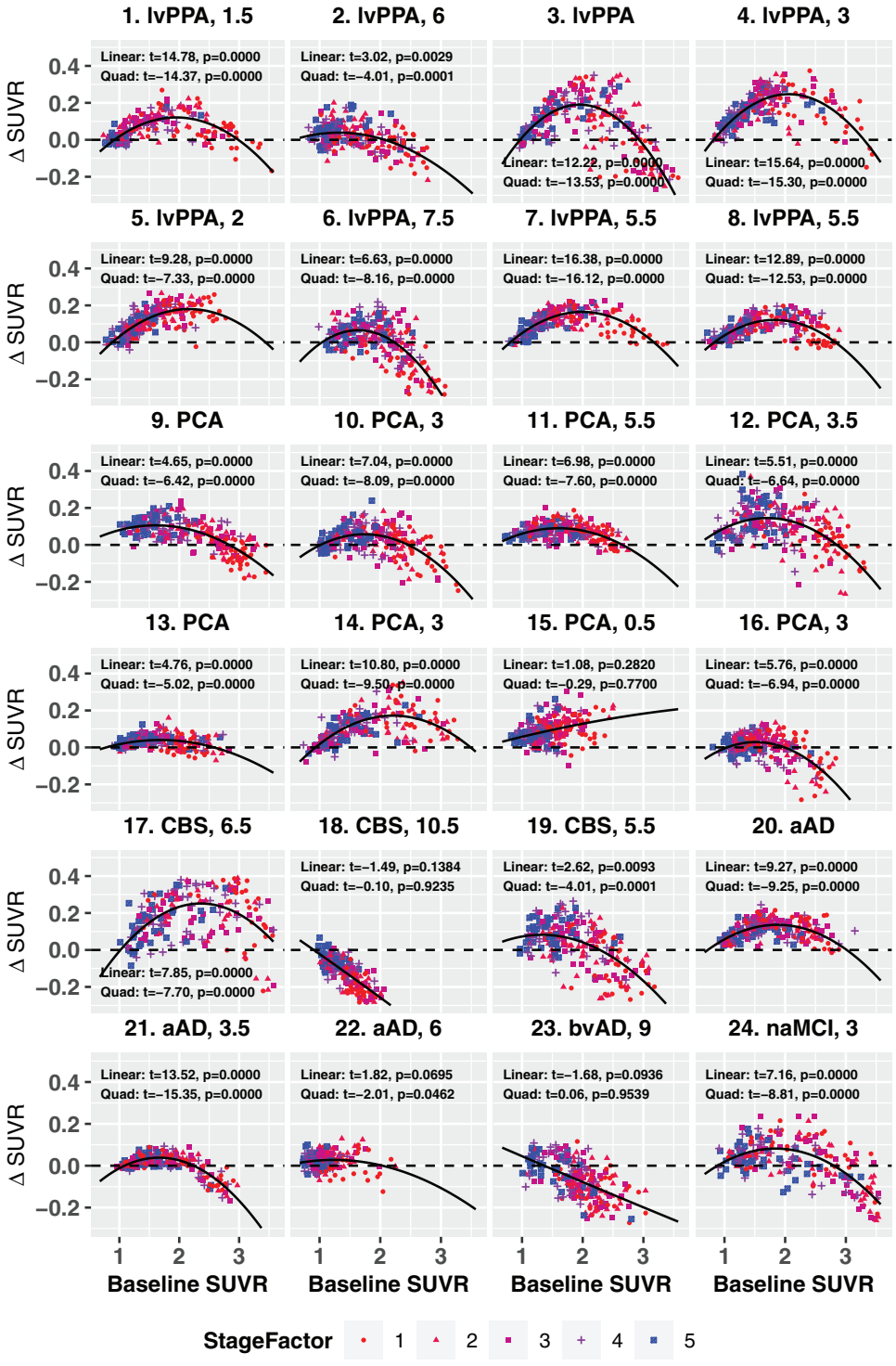


**FIGURE 4** Baseline standardized uptake value ratio (SUVR; uncorrected for partial-volume effects) versus subsequent annualized change for each of 219 regions of interest (ROIs) in each individual. The title of each plot gives the participant number, clinical diagnosis, and total score on the Clinical Dementia Rating scale modified for frontotemporal lobar dementia (FTLD-CDR). The curved line represents the Model 3 fit across the range of observed baseline SUVR values. Data point colors indicate phenotype-specific regional disease stage, according to the magnetic resonance imaging (MRI)-based disease progression models illustrated in Figure 2

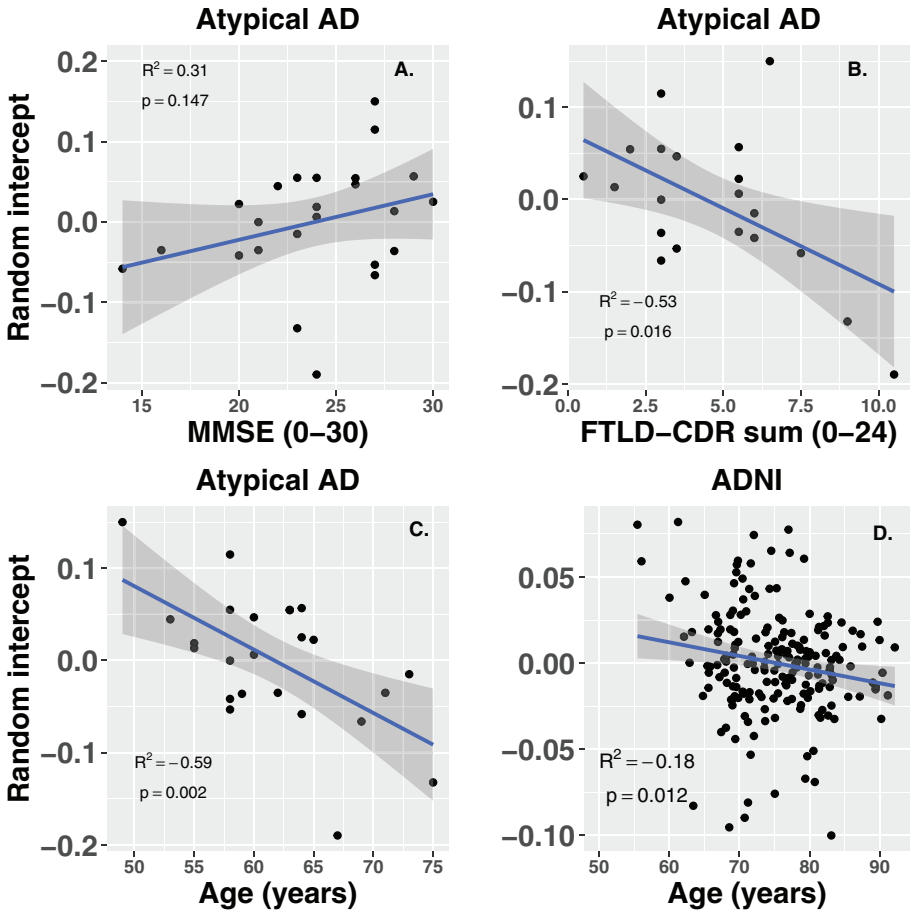


**FIGURE 5** Cognitive impairment and age are associated with inter-individual differences in longitudinal standardized uptake value ratio (SUVR) change. A–C, Cognition and age versus random intercept terms for atypical Alzheimer's disease (AD) patients from Model 3, which relates uncorrected baseline SUVR and its square to annualized SUVR change. D, Alzheimer's Disease Neuroimaging Initiative (ADNI) participants' age versus random intercepts from Model 4

$SUVR_{base}$ (Tables A.16–A.21 in supporting information), and squared residuals for Model 3 (mean: 0.0055; SD = 0.0098) were lower than for Model 5 (mean: 0.0068; SD = 0.0121; mean difference = 0.0013, T[5193] = 12.1, $P < .0001$). For ADNI participants, accuracy did not differ between Model 3 and Model 5. The non-linear relationship between $SUVR_{base}$ and subsequent change persisted using an alternative, eroded white matter reference region (Figure A.1 in supporting information). Head motion was also uncorrelated with ΔSUVR (Figure A.2 in supporting information). These results further suggested plateauing or decreasing of the $^{18}$F-flortaucipir signal was not an artifact of atrophy, sampling, or imaging artifacts.

## 5 | DISCUSSION

To effectively use tau PET as a biomarker and clinical trial endpoint, we must understand how the tau PET signal behaves across clinical variants of AD and over the disease course. The current study investigates potential plateauing or decreases in $^{18}$F-flortaucipir signal change and adds to a scarce literature on longitudinal tau accumulation in atypical AD.[15,16] Areas of early disease identified by phenotype-specific models of atrophy progression exhibited reduced change relative to late-stage disease regions, a finding that generalized between the atypical AD and ADNI samples. Furthermore, in atypical AD, older and more impaired patients exhibited smaller SUVR increases or frank decreases in SUVR, while younger and less impaired patients had greater SUVR increases. A similar age-related reduction in ΔSUVR was observed among ADNI participants.

Additionally, we observed a non-linear relationship between baseline $^{18}$F-flortaucipir uptake and its subsequent change, consistent with the hypothesis that $^{18}$F-flortaucipir has a non-monotonic trajectory in atypical AD. Prior analyses of the association between baseline tau burden and subsequent change have yielded mixed results;[3,15,51] this variability may indicate a complex relationship between past and future tau accumulation that depends on disease severity, clinical characteristics, and brain region. While previous studies attributed $^{18}$F-flortaucipir reductions to measurement error,[4] such error should occur randomly. In contrast, decreases in the current study were predicted by phenotypic disease anatomy, high baseline SUVR, and clinical and demographic factors. Regression to the mean effects were negligible,

and potential confounds such as atrophy, partial-volume effects, and reference region choice could not explain SUVR decreases. We minimized registration error with a longitudinal MRI pipeline using a temporally unbiased template image for each participant.[40] Furthermore, atypical AD patients had predominantly neocortical uptake, which is easier to quantify than Braak stage I–III regions.[9,12] However, even if slowing or decreases in $^{18}$F-flortaucipir uptake relate in part to measurement error, the magnitude and prevalence of such effects may present a challenge to analysis approaches that assume monotonically increasing SUVRs over the disease course.

Rather, observed trajectories of $^{18}$F-flortaucipir signal change in our study may reflect biologically relevant, competing aspects of disease progression. As neurodegeneration accelerates, tau production and aggregation accelerates, but likely will decelerate as neurons dwindle in number. Similar to antibodies used for tau immunohistochemistry, $^{18}$F-flortaucipir binding is also influenced by aggregate maturity[9] and accompanying conformational changes resulting from phosphorylation and truncation events.[52] Tau evolution from pre-tangles into mature tangles could thus result in increasing $^{18}$F-flortaucipir uptake, followed by decreasing uptake with the transition to ghost tangles. Additionally, neurovascular coupling could compound the atrophy effect in advanced disease, as declining regional blood flow could reduce tracer delivery. Thus, the in vivo $^{18}$F-flortaucipir signal may be influenced by overall tau burden and other factors that vary between individuals and over an individual's disease course.

MCI and dementia groups in ADNI demonstrated low levels of baseline tau and longitudinal change. While SUVR thresholds for tau positivity have yet to be established, thresholds of 1.22 to 1.36 in single and composite ROIs have optimally discriminated AD patients from controls.[53–55] Mean cortical $SUVR_{base}$ exceeded this range in atypical AD but not in ADNI; based on recent imaging-pathology correlation studies,[56–58] these results may indicate that most ADNI participants were Braak stage IV or less. Interestingly, in the meta-temporal ROI, the control and MCI groups exhibited modest SUVR increases, but the dementia group did not. Furthermore, longitudinal SUVR change was also reduced in early Braak stage regions for amyloid-positive participants. These results are consistent with the hypothesis of reduced ΔSUVR in advanced tau accumulation. ADNI data did not display the robust non-linear relationship between $SUVR_{base}$ and ΔSUVR observed in atypical AD. This null result is likely related to the generally low SUVR levels, particularly in Braak V–VI regions, and suggests non-linear relationships may be less evident in early-stage typical AD samples like ADNI. However, in single-subject analysis ≈20% of ADNI participants exhibited significant negative associations between $SUVR_{base}$ and ΔSUVR (Table A.35 in supporting information), indicating that plateauing or reduction of tracer uptake occurs in this dataset as well.

Interpretation of our results is constrained by several limitations, including the small atypical AD sample size and that participants only had two $^{18}$F-flortaucipir timepoints. Although single-subject analysis indicated a consistent quadratic association between $SUVR_{base}$ and ΔSUVR in atypical AD, we could not directly test the hypothesis of a non-linear (i.e., first rising, then falling) SUVR trajectory within individuals. The time frame required to observe plateauing or reversal of $^{18}$F-flortaucipir signal change within individuals is unclear and is likely to span several years; future data accrual in longitudinal cohort studies may allow direct evaluation of this hypothesis within individuals. Additionally, the data presented here are based on a single radioligand. However, as other currently available ligands share the same binding sites,[59] comparable results are likely. ADNI had few advanced dementia cases, limiting ability to evaluate late-stage tau dynamics in typical AD. Caution is advised comparing SUVR values from the atypical AD and ADNI samples due to analytic differences; however, we obtained similar results with ADNI data processed using methods applied in the atypical AD sample (Section 10 in supporting information).

In vivo imaging of tauopathy is a promising tool for diagnosis and monitoring of AD neuropathologic change. However, it is important to examine assumptions underlying the analysis and interpretation of tau PET imaging data. The present study discounts several analytic explanations for reductions in $^{18}$F-flortaucipir signal change. Correlations with phenotypic disease anatomy support the hypothesis that the $^{18}$F-flortaucipir signal plateaus or decreases in individuals and brain areas with advanced disease; such changes may complicate parametric interpretation of PET data or its use as a trial endpoint. Instead, the observed changes may result either from decreases in tau accumulation or by biologic changes that affect tracer binding. Further research on how neuropathologic changes and molecular characteristics of tau pathology affect tau PET imaging is warranted to differentiate these possibilities and resolve discrepancies between fluid- and imaging-based measurements of tau pathology.

## ACKNOWLEDGMENTS

Avid Radiopharmaceuticals, Inc. graciously provided $^{18}$F-flortaucipir radioligand for a portion of the scans conducted in this study. The authors would additionally like to thank Quazi Imad Uddin Ibrahim, MSc. of McMaster University for development of methods for bootstrap estimation of regression-to-the-mean effects in non-normal distributions. The authors are grateful for research support from the National Institute on Aging (AG054519, AG017586, AG061277, AG066152, AG058732, AG066597, AG068057, AG063888, AG055005), the National Institute of Neurological Disorders and Stroke (NS109260, NS092091, NS107027), the National Institute on Drug Abuse (DA038726), the Alzheimer's Association (AARF-16-443681), BrightFocus Foundation (A2016244S), the Foundation of the American Society of Neuroradiology, the Commonwealth of Pennsylvania, and the Penn Institute on Aging. ADNI data collection and sharing were funded by National Institutes of Health Grant U01-AG024904 and DOD ADNI (Department of Defense award number W81XWH-12-2-0012). ADNI is funded by the National Institute on Aging, the National Institute of Biomedical Imaging and Bioengineering, and through generous contributions from the following: AbbVie; Alzheimer's Association; Alzheimer's Drug Discovery Foundation; Araclon Biotech; BioClinica, Inc.; Biogen; Bristol-Myers Squibb Company; CereSpir, Inc.; Cogstate; Eisai Inc.; ElanPharmaceuticals, Inc.; Eli Lilly and Company; EuroImmun; F. Hoffmann-La Roche Ltd and its affiliated company Genentech, Inc.; Fujirebio; GE Healthcare; IXICO Ltd.; Janssen Alzheimer Immunotherapy Research & Development, LLC; Johnson & Johnson Pharmaceutical Research &

Development LLC; Lumosity; Lundbeck; Merck & Co., Inc.; Meso Scale Diagnostics, LLC; NeuroRx Research; Neurotrack Technologies; Novartis Pharmaceuticals Corporation; Pfizer Inc.; Piramal Imaging; Servier; Takeda Pharmaceutical Company; and Transition Therapeutics. The Canadian Institutes of Health Research is providing funds to support ADNI clinical sites in Canada. Private sector contributions are facilitated by the Foundation for the National Institutes of Health (www.fnih.org). The grantee organization is the Northern California Institute for Research and Education, and the study is coordinated by the Alzheimer's Therapeutic Research Institute at the University of Southern California. ADNI data are disseminated by the Laboratory for NeuroImaging at the University of Southern California.

## CONFLICTS OF INTEREST

Dr. McMillan has received grants or contracts with Biogen, Inc. and Mitsubishi Tanabe Pharma within the last 36 months; has received consulting fees within the last 36 months from Invicro on behalf of Translational Bioinformatics; is an executive committee member of the Neuroimaging in ALS Society; and is Associate Editor for *NeuroImage: Clinical*. Dr. Irwin is an unpaid member of the Lewy Body Dementia Association Scientific Advisory Council. Dr. Gee has received honoraria or consulting fees within the last 36 months from a talent grant made by the University of Electronic Science and Technology of China, from the Chinese Society of Magnetic Resonance in Medicine & Overseas Chinese Society for Magnetic Resonance in Medicine Joint Meeting, and from the first Annual Scientific Meeting of the Asian Society of Magnetic Resonance in Medicine; has received support for travel and/or meeting attendance within the last 36 months from the Korea Advanced Institute of Science and Technology, the Chinese Society of Magnetic Resonance in Medicine & Overseas Chinese Society for Magnetic Resonance in Medicine Joint Meeting, the first Conference of Chinese Medical Imaging AI, Shanghai, University of Wisconsin, Madison, Michigan Technological University, Annual Shanghai Tech Symposium on Information Science and Technology, the first Annual Scientific Meeting of the Asian Society of Magnetic Resonance in Medicine; and the International Neuroinformatics Coordinating Facility; and has participated on a Data Safety Monitoring Board or Advisory Board within the past 36 months for the Duke Center for In Vivo Microscopy. Dr. Dubroff has received consulting fees from Alcimed, speaking honoraria from Ion Beam Applications (IBA), and consulting fees for his services as an expert reader from Radmetrix within the last 36 months. Dr. Grossman has participated on a Data Safety Monitoring Board or Advisory Board within the past 36 months for the Association for Frontotemporal Degeneration (AFTD). Dr. Nasrallah has received an honorarium from Biogen within the past 36 months. All other authors report that they have no relevant competing interests to disclose.

## ORCID

*Jeffrey S. Phillips* https://orcid.org/0000-0003-0079-9441

## REFERENCES

1. Jagust WJ. Imaging tau pathology—The next step. *JAMA Neurol*. 2020;77:796-797.
2. Matthews D, Ritter A, Thomas RG, et al. The effects of rasagiline on glucose metabolism and cognition and their relationship to Tau burden in a double-blind, placebo-controlled phase Ii Clinical Trial of participants with Alzheimer's Dementia. *SSRN Electronic Journal*. https://doi.org/10.2139/ssrn.3544838
3. Pontecorvo MJ, Devous MD, Kennedy I, et al. A multicentre longitudinal study of flortaucipir (18F) in normal ageing, mild cognitive impairment and Alzheimer's disease dementia. *Brain*. 2019;142:1723-1735.
4. Jack CR, Wiste HJ, Schwarz CG, et al. Longitudinal tau PET in ageing and Alzheimer's disease. *Brain*. 2018;141:1517-1528.
5. Southekal S, Devous MD, Kennedy I, et al. Flortaucipir F 18 quantitation using a Parametric Estimate of Reference Signal Intensity (PERSI). *J Nucl Med*. 2017.
6. Sabuncu MR, Desikan RS, Sepulcre J, et al. The dynamics of cortical and hippocampal atrophy in Alzheimer disease. *Arch Neurol*. 2011;68:1040-1048.
7. Jack CR, DS Knopman, WJ Jagust, et al. Hypothetical model of dynamic biomarkers of the Alzheimer's pathological cascade. *Lancet Neurol*. 2010;9:119-128.
8. Whittington A, Sharp DJ, Gunn RN. Spatiotemporal distribution of $\beta$-amyloid in Alzheimer disease is the result of heterogeneous regional carrying capacities. *J Nucl Med*. 2018;59:822-827.
9. Lowe VJ, Curran G, Fang P, et al. An autoradiographic evaluation of AV-1451 Tau PET in dementia. *Acta Neuropathologica Communications*. 2016;4.
10. Horie K, Barthélemy NR, Sato C, Bateman RJ. CSF tau microtubule binding region identifies tau tangle and clinical stages of Alzheimer's disease. *Brain*. 2021;144:515-527.
11. Murray ME, Graff-Radford NR, Ross OA, Petersen RC, Duara R, Dickson DW. Neuropathologically defined subtypes of Alzheimer's disease with distinct clinical characteristics: a retrospective study. *Lancet Neurol*. 2011;10:785-796.
12. Baker SL, Maass A, Jagust WJ. Considerations and code for partial volume correcting [18F]-AV-1451 tau PET data. *Data in Brief*, 2017;15:648-657. https://doi.org/10.1016/j.dib.2017.10.024
13. Phillips JS, Da Re F, Dratch L, et al. Neocortical origin and progression of gray matter atrophy in nonamnestic Alzheimer's disease. *Neurobiol Aging*. 2018;63:75-87.
14. Phillips JS, Da Re F, Irwin DJ, et al. Longitudinal progression of grey matter atrophy in non-amnestic Alzheimer's disease. *Brain*. 2019;142:1701-1722.
15. Sintini I, Martin PR, Graff-Radford J, et al. Longitudinal tau-PET uptake and atrophy in atypical Alzheimer's disease. *NeuroImage: Clinical*. 2019;23.
16. Sintini I, Graff-Radford J, Senjem ML, et al. Longitudinal neuroimaging biomarkers differ across Alzheimer's disease phenotypes. *Brain*. 2020;143:2281-2294.
17. Ossenkoppele R, Pijnenburg YAL, Perry DC, et al. The behavioural/dysexecutive variant of Alzheimer's disease: clinical, neuroimaging and pathological features. *Brain*. 2015;138:2732-2749.
18. Cho H, Jeon S, Kang SJ, et al. Longitudinal changes of cortical thickness in early- versus late-onset Alzheimer's disease. *Neurobiol Aging*. 2013;34:e9-e15.
19. Balasa M, Gelpi E, Antonell A, et al. Clinical features and APOE genotype of pathologically proven early-onset Alzheimer disease. *Neurology*. 2011;76:1720-1725.
20. Mendez MF, Lee AS, Joshi A, Shapira JS. Nonamnestic presentations of early-onset Alzheimer's disease. *Am J Alzheimers Dis and Other Demen*. 2012;27:413-420.
21. Dickerson B, McGinnis SM, Xia C, et al. Approach to atypical Alzheimer's disease and case studies of the major subtypes. *CNS Spectr*. 2017;22:439-449.
22. Braak H, Braak E. Neuropathological stageing of Alzheimer-related changes. *Acta Neuropathol (Berl)*. 1991;82:239-259.
23. Irwin DJ, McMillan CT, Toledo JB, et al. Comparison of cerebrospinal fluid levels of tau and A$\beta$ 1-42 in Alzheimer disease and frontotemporal

degeneration using 2 analytical platforms. *Arch Neurol*. 2012;69:1018-1025.
24. Cousins KAQ, Irwin DJ, Wolk DA, et al. ATN status in amnestic and non-amnestic Alzheimer's disease and frontotemporal lobar degeneration. *Brain*. 2020;143:2295-2311.
25. Gorno-Tempini ML, Hillis AE, Weintraub S, et al. Classification of primary progressive aphasia and its variants. *Neurology*. 2011;76:1006-1014.
26. Giannini LA, Irwin DJ, McMillan CT, et al. Clinical marker for Alzheimer disease pathology in logopenic primary progressive aphasia. *Neurology*. 2017;88:2276-2284.
27. Crutch SJ, Schott JM, Rabinovici GD, et al. Consensus classification of posterior cortical atrophy. *Alzheimers Dement*. 2017;13:870-884.
28. Rascovsky K, Hodges JR, Knopman D, et al. Sensitivity of revised diagnostic criteria for the behavioural variant of frontotemporal dementia. *Brain*. 2011;134:2456-2477.
29. Armstrong MJ, Litvan I, Lang AE, et al. Criteria for the diagnosis of corticobasal degeneration. *Neurology*. 2013;80:496-503.
30. Lee SE, Rabinovici GD, Mayo MC, et al. Clinicopathological correlations in corticobasal degeneration. *Ann Neurol*. 2011;70:327-340.
31. Medaglia JD, Huang W, Segarra S, et al. Brain network efficiency is influenced by the pathologic source of corticobasal syndrome. *Neurology*. 2017;89:1373-1381.
32. Spotorno N, McMillan CT, Powers JP, Clark R, Grossman M. Counting or Chunking? Mathematical and heuristic abilities in patients with corticobasal syndrome and posterior cortical atrophy. *Neuropsychologia*. 2014;64:176-183.
33. McKhann GM, Knopman DS, Chertkow H, et al. The diagnosis of dementia due to Alzheimer's disease: recommendations from the National Institute on Aging-Alzheimer's Association workgroups on diagnostic guidelines for Alzheimer's disease. *Alzheimers Dement*. 2011;7:263-269.
34. Albert MS, DeKosky ST, Dickson D, et al. The diagnosis of mild cognitive impairment due to Alzheimer's disease: recommendations from the National Institute on Aging-Alzheimer's Association workgroups on diagnostic guidelines for Alzheimer's disease. *Alzheimers Dement*. 2011;7:270-279.
35. Nasrallah IM, Chen YJ, Hsieh M-K, et al. 18F-flortaucipir PET/MRI correlations in nonamnestic and amnestic variants of Alzheimer disease. *J Nucl Med*. 2018;59:299-306.
36. Phillips JS, Das SR, McMillan CT, et al. Tau PET imaging predicts cognition in atypical variants of Alzheimer's disease. *Hum Brain Mapp*. 2018;39:691-708.
37. Folstein MF, Folstein SE, McHugh PR. "Mini-mental state": a practical method for grading the cognitive state of patients for the clinician. *J Psychiatr Res*. 1975;12:189-198.
38. Knopman DS, Kramer JH, Boeve BF, et al. Development of methodology for conducting clinical trials in frontotemporal lobar degeneration. *Brain*. 2008;131:2957-2968.
39. Morris JC. The Clinical Dementia Rating (CDR): current version and scoring rules. *Neurology*. 1993;43:2412-2414.
40. Tustison NJ, Holbrook AJ, Avants BB, et al. Longitudinal Mapping of Cortical Thickness Measurements: an Alzheimer's Disease Neuroimaging Initiative-Based Evaluation Study. *J Alzheimers Dis*. 2019;71:165-183.
41. Avants B, Cook PA, McMillan C, et al. Sparse Unbiased Analysis of Anatomical Variance in Longitudinal Imaging. *Med Image Comput Comput Assist Interv*. 2010;13:324-331.
42. Diedrichsen J, Balsters JH, Flavell J, Cussans E, Ramnani N. A probabilistic MR atlas of the human cerebellum. *Neuroimage*. 2009;46:39-46.
43. Diedrichsen J, Maderwald S, Küper M, et al. Imaging the deep cerebellar nuclei: a probabilistic atlas and normalization procedure. *Neuroimage*. 2011;54:1786-1794.
44. Thomas BA, Cuplov V, Bousse A, et al. PETPVC: a toolbox for performing partial volume correction techniques in positron emission tomography. *Phys Med Biol*. 2016;61:7975.
45. Cammoun L, Gigandet X, Meskaldji D, et al. Mapping the human connectome at multiple scales with diffusion spectrum MRI. *J Neurosci Methods*. 2012;203:386-397.
46. Hagmann P, Cammoun L, Gigandet X, et al. Mapping the structural core of human cerebral cortex. *PLoS Biol*. 2008;6:e159.
47. R LaJoie, Perrotin A, de LaSayetteV, et al. Hippocampal subfield volumetry in mild cognitive impairment, Alzheimer's disease and semantic dementia. *NeuroImage: Clinical*. 2013;3:155-162.
48. Landau S, Ward TJ, Murphy A & Jagust W Flortaucipir (AV-1451) processing methods 2021.
49. Galton F. Regression towards mediocrity in hereditary stature. *JRAI*. 1886;15:246-263.
50. Barnett AG, Pols JC, Dobson AJ. Regression to the mean: what it is and how to deal with it. *Int J Epidemiol*. 2005;34:215-220.
51. Chiotis K, Saint-Aubert L, Rodriguez-Vieitez E, et al. Longitudinal changes of tau PET imaging in relation to hypometabolism in prodromal and Alzheimer's disease dementia. *Mol Psychiatry*. 2018;23:1666-1673.
52. Binder LI, Guillozet-Bongaarts AL, Garcia-Sierra F, Berry RW. Tau, tangles, and Alzheimer's disease. *Biochim Biophys Acta*. 2005;1739:216-223.
53. Ossenkoppele R, Rabinovici GD, Smith R, et al. Discriminative accuracy of [18F]flortaucipir positron emission tomography for Alzheimer Disease vs other neurodegenerative disorders. *JAMA*. 2018;320(11):1151-1162. https://doi.org/10.1001/jama.2018.12917
54. Schwarz AJ, Yu P, Miller BB, et al. Regional profiles of the candidate tau PET ligand 18F-AV-1451 recapitulate key features of Braak histopathological stages. *Brain*. 2016;139:1539-1550.
55. Meyer P-F, Pichet Binette A, Gonneaud J, Breitner JCS, Villeneuve S. Characterization of Alzheimer disease biomarker discrepancies using cerebrospinal fluid phosphorylated tau and AV1451 positron emission tomography. *JAMA Neurol*. 2020;77:508-516.
56. Lowe VJ, Lundt ES, Albertson SM, et al. Tau-positron emission tomography correlates with neuropathology findings. *Alzheimers Dement*. 2020;16:561-571.
57. Fleisher AS, Pontecorvo MJ, Devous MD, et al. Positron emission tomography imaging with [18F]flortaucipir and postmortem assessment of Alzheimer Disease neuropathologic changes. *JAMA Neurol*, 2020;77(7):829. https://doi.org/10.1001/jamaneurol.2020.0528
58. Soleimani-Meigooni DN, Iaccarino L, La Joie R, et al. 18F-flortaucipir PET to autopsy comparisons in alzheimer's disease and other neurodegenerative diseases. *Brain*. 2020;143:3477-3494.
59. Murugan NA, Nordberg A, Ågren H. Different Positron Emission Tomography Tau Tracers Bind to Multiple Binding Sites on the Tau Fibril: insight from Computational Modeling. *ACS Chem Neurosci*. 2018;9:1757-1767.

## SUPPORTING INFORMATION

Additional supporting information may be found in the online version of the article at the publisher's website.

**How to cite this article:** Phillips JS, Nitchie IV FJ, Da Re F, et al. Rates of longitudinal change in $^{18}$F-flortaucipir PET vary by brain region, cognitive impairment, and age in atypical Alzheimer's disease. *Alzheimer's Dement*. 2022;18:1235–1247. https://doi.org/10.1002/alz.12456